

One-Dimensional Cold Cap Model for Melters with Bubblers

Richard Pokorný,^{‡,†} Zachary J. Hilliard,[§] Derek R. Dixon,[§] Michael J. Schweiger,[§] Donna P. Guillen,[¶] Albert A. Kruger,^{||} and Pavel Hrma[§]

[‡]Department of Chemical Engineering, University of Chemistry and Technology Prague, 166 28 Prague 6, Czech Republic

[§]Pacific Northwest National Laboratory, Richland, Washington 99352

[¶]Idaho National Laboratory, Idaho Falls, Idaho 83415

^{||}U.S. Department of Energy, Office of River Protection, Richland, Washington 99352

The rate of glass production during vitrification in an all-electrical melter greatly impacts the cost and schedule of nuclear waste treatment and immobilization. The feed is charged to the melter on the top of the molten glass, where it forms a layer of reacting and melting material, called the cold cap. During the final stages of the batch-to-glass conversion process, gases evolved from reactions produce primary foam, the growth and collapse of which controls the glass production rate. The mathematical model of the cold cap was revised to include functional representation of primary foam behavior and to account for the dry cold cap surface. The melting rate is computed as a response to the dependence of the primary foam collapse temperature on the heating rate and melter operating conditions, including the effect of bubbling on the cold cap bottom and top surface temperatures. The simulation results are in good agreement with experimental data from laboratory-scale and pilot-scale melter studies. The cold cap model will become part of the full three-dimensional mathematical model of the waste glass melter.

I. Introduction

GLASS batch melting has been investigated for many decades to gain a deeper understanding of the process and to optimize the glass melting furnace design and operation.¹ For the vitrification of radioactive wastes, the rate of melting is one of the major concerns. An increased melting rate can significantly reduce costs and shorten the life cycle of the cleanup process at the Hanford Site in Washington State, USA, where more than 200 000 m³ of nuclear waste will be vitrified over the next few decades.²

Sophisticated mathematical models have been developed and successfully applied in recent decades to reduce the unit cost of manufacturing, optimize the stringent quality requirements, and design new products and processes.³ Regrettably, as Choudhary pointed out,³ the modeling of phenomena in the batch melting subdomain still represents a relatively weak link in the glass furnace modeling effort. Because the batch melting influences the velocity and temperature fields inside the entire furnace,⁴ furnace models cannot reliably predict the melting rate without an adequate model for batch melting kinetics.

Following Freeman's pioneering study,⁵ Pokorný and Hrma,^{6,7} recently developed a model of the cold cap (or the

batch blanket) that solves the issue of heat transfer in the cold cap and incorporates the dynamic behavior of the foam layer, through which the heat is transferred from the melt pool. The model was formulated for the situation in which the flow in the melt pool occurs by natural convection and the top surface of the cold cap is covered by boiling slurry.

The natural convection in the molten glass below the cold cap is driven by buoyancy, which is governed by the density gradient associated with the temperature gradient, but weakened by the presence of gas bubbles that are continuously produced in the melt. Under these conditions, a triple layer of foam forms under the cold cap, consisting of primary foam, cavities, and secondary foam.⁷ Primary foam arises when enough glass-forming melt is produced within the glass batch (or melter feed) that the viscous liquid becomes continuous and gas can no longer escape through open pores. Secondary foam is an accumulation of bubbles rising from the melt below the cold cap. Primary foam bubbles are carried down by the viscous melt and coalesce into cavities, to which secondary foam merges from below. The cavities, or the gas in the cavities, move horizontally and escape to the plenum space on the cold cap edges or through vent holes. This triple layer of foam represents a formidable resistance to heat transfer. The necessity to transfer the heat for slurry evaporation, in addition to the batch melting heat, further hinders the melting process.

The introduction of bubblers recently revolutionized the waste glass melting industry.^{8,9} Bubblers have been used by commercial glassmakers for many decades in gas-heated glass melting furnaces, but solely for controlling the melt flow,¹⁰ not as a means for enhancing the rate of melting. Bubbling gas into the melt pool under the cold cap introduces forced convection several times more powerful than the buoyancy-driven natural convection. The forced convection driven by a jet of bubbles homogenizes the melt thermally, thus bringing hot melt directly to the cold cap. Furthermore, it also prevents formation of secondary foam and removes sluggish or stagnant large cavities, so the primary foam layer under the cold cap comes in direct contact with molten glass¹¹ [Fig. 1(a)]. The recent study of melting high-level waste (HLW) glass feeds with various sources of iron¹² in a research-scale melter equipped with a bubbler found the glass virtually fully oxidized with the Fe(II)/Fe fraction of 10^{−4}, whereas crucible melts typically show the values of 0.03¹³. This indicates that the O₂ bubbles remained dispersed in the melt and Fe(II) reoxidized on cooling.

With secondary foam and cavities virtually absent, the heat-transfer resistance of the foam layer is greatly decreased. Moreover, slurry feed cannot spread beyond the vent holes and fissures in the cold cap. As a result, the majority of the cold cap upper surface is dry. The increased surface temperature causes the feed to prereact to some extent, thus reducing

E. Vance—contributing editor

Manuscript No. 36596. Received March 19, 2015; approved June 23, 2015.

[†]Author to whom correspondence should be addressed. e-mail: richard.pokorny@vscht.cz

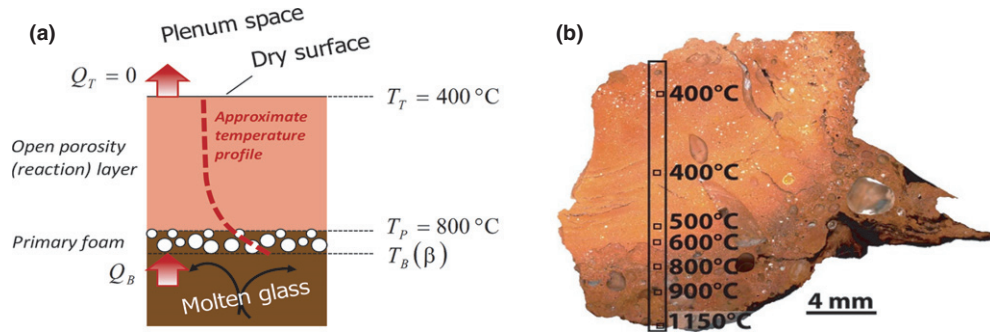


Fig. 1. (a) Schematic 1D illustration of a cold cap floating on a pool of molten glass (left); (b) the polished cold cap section obtained from laboratory-scale melter experiment (right).¹⁹ The schematics also depict the boundary layer temperatures (T_T , T_P , and T_B) and boundary heat fluxes (Q_U and Q_B).

the heat flux necessary to be transferred through the cold cap bottom. Consequently, the rate of melting increased several times.^{8,14}

Accordingly, bubbling changes the boundary conditions for both top and bottom surfaces in the cold cap model. The direct contact with molten glass affects the dynamic behavior of primary foam and, hence, the cold cap bottom temperature. This requires reexamining the concept of uniform melting temperature¹⁵ in favor of relating the cold cap bottom temperature to the growth and collapse of primary foam as the terminal conversion process.¹⁶ The gas is released into horizontally moving cavities that are swiftly carried away by convection. The cold cap bottom is thus a surface below which the melt porosity is virtually zero (ignoring sporadic bubbles) and the vertically descending material joins the circulation in the melt pool.

The structure of the cold cap is described in Section II, in which we also present the experimental approach to the primary foam evolution and decay. The simulation results are presented in Section III, along with a comparison with available experimental data from laboratory-scale and pilot-scale melter studies. This is the first time that the model-estimated temperature profile has been compared with an experimentally determined temperature distribution within the cold cap. However, only after the cold cap model implementation into the glass melter model is accomplished,¹⁷ can the melting rate ultimately be estimated both as a function of the feed formulation and melter operating conditions.

Although the cold cap model inevitably rests on data obtained for a particular waste stream, this paper is focused on the model development, which makes the methodology applicable wherever primary foaming occurs, including commercial glass melting.

II. Theory and Experimental

(1) Cold Cap Structure

The conversion of batch (or melter feed) to glass occurs in the cold cap, a layer of reacting material floating on the top of molten glass. As in our previous work,^{6,7,11} the present cold cap model rests on two simplifying assumptions. First, it is assumed that all feed components and evolving gases move, and that the heat flows in the vertical direction. Thus, horizontal mass and heat flows are omitted. This assumption allows us to treat the feed-to-glass conversion within the cold cap as a 1-D problem. Second, we assume that all solids and liquids (molten salts and glass-forming melt) move with the same velocity. This allows us to treat the solid and liquid phases as a single condensed phase. Phenomena such as the reflux of volatiles or drainage of low-viscosity melt are not represented.

Figure 1(a) illustrates the cold cap, consisting of two main regions, an open porosity layer and the primary foam. As explained above, cavities and secondary foam are displaced by the powerful forced convection driven by bubbling. Moreover, based on recent laboratory-scale and pilot-scale cold

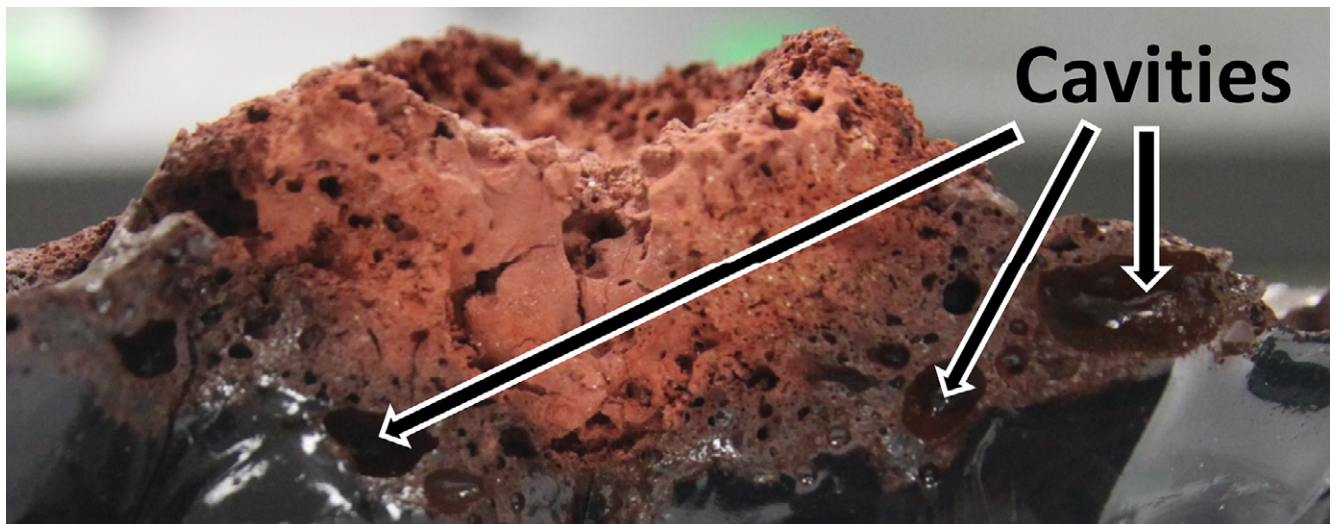


Fig. 2. Section of a small cold cap from laboratory-scale melter experiment. No bubbling was applied. The quenched sample shows the boundary between primary foam and molten glass, along which the primary foam collapses into cavities, which move sideways until they can escape into the atmosphere.

cap observations, which indicate that most of the cold cap surface is dry, we considered a case with the top surface temperature (T_T) higher than $\sim 100^\circ\text{C}$.¹⁸ Based on laboratory-scale melter experiments, the T_T can be as high as $\sim 400^\circ\text{C}$ ¹⁹ [Fig. 1(b)]. With boiling slurry on the top surface, the cold cap thickness is limited because of the heat flux needed to evaporate the water from slurry. When the water is evaporated and the melter feed partially preheated by the heat flux from the plenum space, the cold cap thickness is no longer constrained and a feed material of a constant temperature can accumulate in the upper part of the cold cap (Fig. 1). Thus, the thickness of the cold cap can grow, and is restricted solely by the feeding rate and feed rheology.²⁰

Most of the batch gases evolve in the upper layer of the cold cap, from which they freely escape through open pores. At the primary foam temperature, T_P , open porosity closes as the glass-forming melt is sufficiently abundant to become connected. The first bubbles, initially of irregular shape (Fig. 2), appear in the melt that encapsulates undissolved solids. Because of the high viscosity of the melt, the buoyant upward motion of the bubbles is slower than the downward motion of the melt.⁶ While the bubbles move down, they continue to grow, as a result of continuing gas-evolving reactions, increasing temperature, and coalescence, until their size is large enough and viscosity low enough that their downward motion stops and the primary foam starts to collapse, releasing gas into horizontally moving cavities (Fig. 2). Thus, foam ceases to exist at the cold cap bottom temperature, T_B , and the molten feed merges with the circulating molten glass below the cold cap.

(2) Primary Foam as the Terminal Conversion Process

In this work, we suggest that the terminal batch-to-glass conversion process, which determines the cold cap bottom, is the progress of growth and the collapse of primary foam. Figure 3 shows the results of pellet (pressed dry feed) expansion experiments conducted with a simplified version of a high-alumina HLW melter feed originally designed for the Hanford Waste Treatment and Immobilization Plant.^{21,22} As the temperature rises above the primary foam temperature, T_P , which depends on the feed composition and its time-temperature history during heating,²³ the feed starts to expand. Expansion continues until the gas-phase release exceeds its accumulation, at which point the volume shrinks, terminating in a bubble-free melt at the primary foam collapse temperature, T_M (Fig. 3).

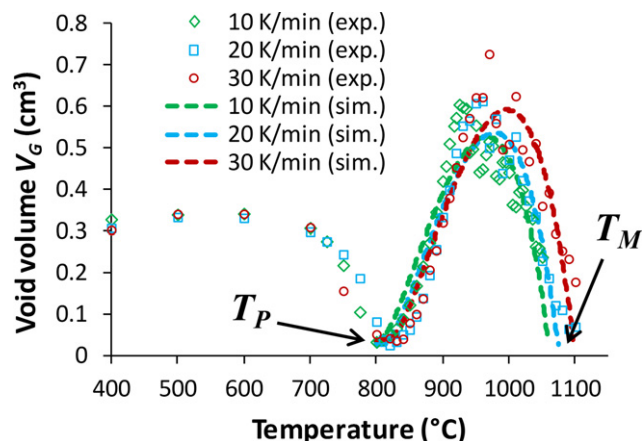


Fig. 3. Gas phase volume, V_G , versus temperature measured for various heating rates of melter feed pellets. Points represent the measured values, dashed lines the simulated expansion and collapse; T_P and T_M correspond to the primary foam and foam collapse temperatures, respectively.

In the cold cap, primary foam collapses at T_B [Fig. 1(a)], at which point the melt is practically free of bubbles and the feed is nearly fully converted to molten glass, with the exception of the continuation of inhomogeneities attenuating and residual solids dissolving while the melt is circulating in the melt pool.

(3) Kinetic Model for Primary Foam

The kinetics of primary foam evolution and decay has been studied using volume expansion experiments with the feed^{24–27} and can be expressed in the form of the gas-phase balance

$$\frac{dV_G}{dt} = R_E - R_C \quad (1)$$

where V_G is the volume of gas in the foam, t is time, R_E is the gas generation rate (leading to foam expansion), and R_C is the gas release rate to the atmosphere (governing foam collapse). In the case of monitoring the volume of a feed pellet, dV_G/dt is the rate of change in the pellet void volume (Fig. 3).

An n th order kinetic model for gas-evolving reactions has been developed, but could only be validated up to 825°C ²⁸ because the thermogravimetric response begins to fluctuate when the feed turns into foam. Moreover, the n th order kinetic model is not suitable for the description of gas evolution in the foam, as the gas is continually evolving above T_P due to redox reactions. Three sources of foam expansion exist: residual batch gases, thermal expansion of existing gases, and oxygen generation from redox reactions. The tail of the last batch reaction, producing a minor amount of CO_x or NO_x , is probably not the most powerful source of foaming. Considering the ideal gas law, the increased temperature from 800°C to 940°C is responsible for about 13% of gas volume expansion. Gradual reduction in Fe_2O_3 to FeO provides a steady source of oxygen. Unlike batch reactions, which are mainly controlled by diffusion between phases, the redox reactions in the melt run fast and are in, or close to, equilibrium. The melt contains 5.73 mass% Fe_2O_3 .⁷ Considering that $\ln[\text{Fe(III)}/\text{Fe(II)}] = A - B_{\text{Fe}}/T$, where $A = 5.05$ and $B_{\text{Fe}} = 1.21 \times 10^4 \text{ K}$,²² 0.3% of Fe(III) is reduced to Fe(II) between 800°C and 900°C , producing 50 mL of O_2 per kg of glass. This corresponds to $\sim 13.2 \text{ vol\%}$ of bubble-free melt. Considering the oxygen release and ongoing batch reactions as a relatively steady source of gas over the temperature interval of foaming, we chose the arctan function to describe the continuous gas evolution above T_P .

The gas release rate is controlled by the thinning of the liquid films that separate the foam bubbles, leading to coalescence (internal collapse) and opening the foam cells to the atmosphere. The main factor that destabilizes the films separating bubbles from each other and from the atmosphere is the decrease in viscosity resulting from increasing temperature. Solid particles and compositional nonuniformity also affect the film stability. Thus, the collapse rate should be inversely proportional to viscosity η .^{29,30}

Although a detailed mathematical description of foam evolution and decay would be exceedingly complex,³¹ experimental data can be sufficiently represented by the empirical equation

$$\frac{dV_G}{dT} = b_1 \arctan \left[\frac{T - T_1}{T_2} \right] - b_2 \exp \left(-\frac{B}{T} \right) \quad (2)$$

where T is the temperature, and b_1 , b_2 , T_1 , T_2 , and B are parameters for the gas evolution (1st term on the right side of Eq. (2)) and gas release [2nd term on the right side of Eq. (2)]. This equation was fitted to the foam evolution and decay data obtained between 800°C – 1100°C ; only T_1 and b_2

Table I. Kinetic Parameters Obtained by Fitting of Eq. (2) to Data

		10 K/min	20 K/min	30 K/min
Foam growth	b_1 (m ³ K ⁻¹)		4.83×10^{-3}	
	T_1 (K)	1070	1079	1088
	T_2 (K)		20.74	
Foam collapse	b_2 (m ³ K ⁻¹)	3.10×10^{-5}	2.70×10^{-5}	2.19×10^{-5}
	B (K)		18343	

Parameters T_1 and b_2 were allowed to vary with heating rate, whereas parameters b_1 , T_2 , and E were kept constant.

parameters were allowed to vary with the heating rate. The results of parameter fitting are summarized in Table I and displayed in Fig. 3 with dashed lines. Note that the value of B is practically the same as in the viscosity–temperature relationship,³² indicating that the foam collapse is indeed inversely proportional to viscosity.

(4) Cold Cap Model

The employed model⁷ solves the energy balance within the cold cap,

$$\rho_b c_b \frac{dT}{dt} = (j_b c_b^{\text{Eff}} - j_g c_g) \frac{dT}{dx} - \lambda^{\text{Eff}} \frac{d^2 T}{dx^2} \quad (3)$$

where ρ is the spatial density, c is the effective heat capacity, j is the mass flux, λ is the heat conductivity, x is the spatial coordinate (vertical position), and the subscripts b and g denote the condensed phase and the gas phase, respectively. The effective heat capacity of the condensed phase, c_b^{Eff} , includes the heat from melting reactions (such as the evaporation of bonded water and the decomposition of carbonates). The effective heat conductivity, λ^{Eff} , is assumed to involve both conductive and radiative modes of heat transfer in the feed. The condensed phase mass flux within the cold cap is calculated as $j_b = \alpha_b j_T$, where α_b is the mass fraction of the condensed phase and j_T is the mass flux of the dry feed entering the cold cap.

Our previous studies^{7,33,34} present the feed properties necessary for the solution of Eq. (3) [i.e., $\rho(T)$, $c(T)$, $\alpha_b(T)$, and $\lambda^{\text{Eff}}(T)$] as functions of temperature. Because of the absence of the cavity layer and the secondary foam, the $\rho(T)$ and $\lambda^{\text{Eff}}(T)$ functions were modified for $T > T_p$. The bulk density (Fig. 4) was evaluated based on feed expansion experiments (Fig. 3). For simplicity, we used $\lambda^{\text{Eff}} = 0.5 \text{ W} \cdot (\text{m} \cdot \text{K})^{-1}$ for $T > 800^\circ\text{C}$ (Fig. 4), a constant value that is equal to the average λ^{Eff} in the primary foam region.³⁴

The energy balance equation, Eq. (3), was solved using the finite volume method³³ with 500 finite volumes. Considering

the average cold cap thickness of ~ 3 cm, the discretization step was ~ 0.06 mm. The algorithm was coded in Mathworks® (Natick, MA) MATLAB7.

(5) Implementation of Primary Foam into the Cold Cap Model

Naturally, differences exist between foam evolution and decay in the cold cap and in the pellet. In the cold cap, the melt moves down through the foam layer, whereas the shape of pellets changes under the influence of capillary and gravity forces. In both the cold cap and the pellet, the open porosity closes and the feed turns into foam at T_p . At T_B , the primary foam in the cold cap collapses into cavities, whereas the pellet foam cells open to the atmosphere at T_M (Fig. 3). We assume that foam cells collapsing into cavities and into the atmosphere are equivalent processes, thus $T_B = T_M$. As the T_M depends on the heating rate, or, more precisely, the time-temperature history experienced by the feed, it follows that the temperature at which the foam collapses in the cold cap, T_B , is related to the heating rate in the same way as in the pellet.

Hence, the bottom boundary condition is given by the $T_M(\beta)$ function, where β is associated with the heat and mass flux in the cold cap. An increase in the average heating rate in the cold cap would result in a higher T_B and foam accumulation that would decrease the heat flux to the cold cap and slow down the melting rate, thus reestablishing the steady state. If, on the contrary, the heating rate in the cold cap decreased, a lower T_B would allow a faster heat flux to the cold cap, resulting in faster melting and a higher heating rate, again reestablishing the steady state.

The biggest advantage of this simple model is that it avoids the development of complex relationships for the structure and heat transfer in the primary foam region, allowing the transition of the feed into molten glass to be represented by the pellet test experiments, while disregarding secondary phenomena.

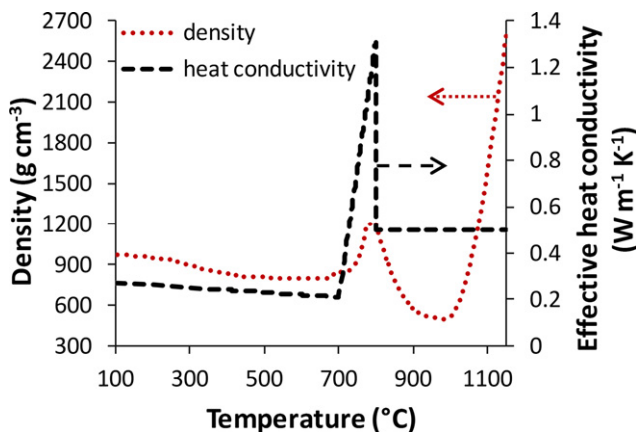


Fig. 4. Melter feed density and effective heat conductivity versus temperature.

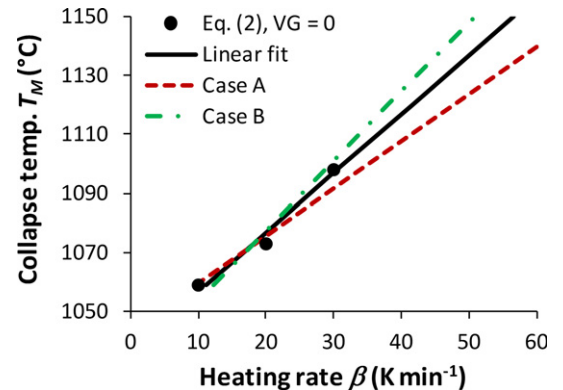


Fig. 5. Relationship between the collapse temperature, T_M , and heating rate, β , evaluated from Fig. 3 (black points). The solid line represents linear fit to data. The dashed and dash-dotted lines (Cases A and B) show other possible $T_M(\beta)$ relationships used for the parametrical study in Section III.

Figure 5 displays the relationship between the heating rate, β , and the T_M , the temperature at which the dashed lines in Fig. 2 intersect the horizontal axis, which was computed by integrating Eq. (2) and setting $V_G = 0$. The $T_M(\beta)$ relationship is assumed to be linear (mainly due to the lack of more than three data points) and extrapolated to higher rates of heating that occur in the cold cap, but were not accessible in the equipment used for the pellet expansion monitoring. As it is possible that the $T_M(\beta)$ line could have a different slope if more data were available (possibly resulting in somewhat different coefficient values that would be shown in Table I), as well as for the sake of model sensitivity to experimental parameters, hypothetical Cases A and B (Fig. 5) were considered, to study different heating rate dependence on T_M .

(6) Model Iteration

The iterative procedure for the calculation of the melting rate by the cold cap model including the primary foam is as follows:

1. The boundary conditions T_T and T_B are supplied to the cold cap model. These temperatures will naturally be determined when the cold cap model will become a part of the glass melter model, which is currently being developed at Idaho National Laboratory.³⁵
2. Considering the dry cold cap surface and $Q_T = 0$ (all heat coming from below is consumed inside the cold cap), an initial melting rate is guessed and the corresponding cold cap thickness is calculated. The initial melting rate assessment was varied within the range of expected results ($1000\text{--}2000\text{ kg m}^{-2}\text{ day}^{-1}$); its value affected the simulation (convergence) speed, not the final result.
3. The average heating rate of the feed is calculated from the obtained time-temperature history of the feed in the cold cap. The average heating rate experienced by the feed in the cold cap was computed using the temperature interval between 500°C and T_P , at which most of the gas evolves.²⁸
4. The primary foam collapse temperature, T_M , corresponding to the average heating rate is evaluated (see Fig. 5) and compared to the set boundary condition at the cold cap bottom, T_B .
5. The melting rate is iterated until T_M equals T_B , indicating that a steady-state melting rate was reached.

III. Results and Discussion

(1) Effect of Cold Cap Top Temperature on Melting Rate

Bubbling creates vent holes in the cold cap, where the slurry feed comes into a direct contact with molten glass. Thus,

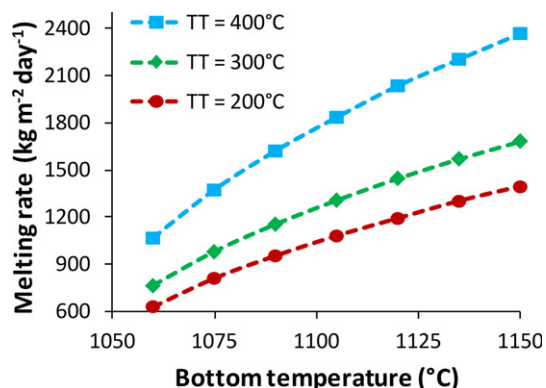


Fig. 6. Melting rate versus cold cap bottom temperature, T_B , for various values of cold cap top temperature, T_T .

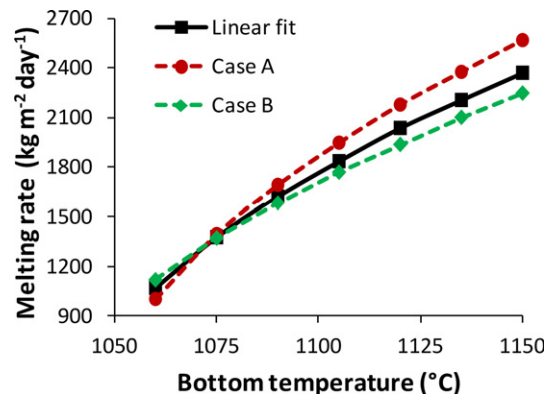


Fig. 7. Melting rate versus cold cap bottom temperature for $T_M(\beta)$ functions displayed in Fig. 5 ($T_T = 400^\circ\text{C}$).

water quickly evaporates and leaves only a fraction of the cold cap surface covered by slurry. The dry feed surface can then be heated to higher temperatures. The T_T will eventually be estimated when the cold cap model is implemented into the model of the glass melter. For now, we need to assess the realistic range for the T_T values. Dixon et al.¹⁹ reported that the temperature at the top of the cold cap in a laboratory-scale melter was $T_T = 400^\circ\text{C}$. Guerrero et al.^{36,37} calculated the temperature at the top of the cold cap in the Defense Waste Processing Facility melter, which is equipped with upper heaters, to be between 450°C and 477°C . Even without upper heaters, the plenum temperature in melters equipped with bubblers can be as high as 550°C .¹⁸ Figure 6 displays the simulation results calculated for T_T values between 200°C and 400°C to cover the possible range of cold cap surface temperatures, showing that the melting rate strongly increases with increasing T_T and T_B , reaching up to $\sim 2500\text{ kg m}^{-2}\text{ day}^{-1}$.

The increase in the melting rate with the T_B well agrees with experimental observations that report faster melting rates for higher melter operating temperatures and increased bubbling, as both of these effects increase the temperature directly at the cold cap bottom.^{18,38} According to pilot-plant data, bubbling increased the melting rate to as high as $2200\text{ kg m}^{-2}\text{ day}^{-1}$.³⁸ A better comparison will be provided once the cold cap model is implemented into the melter model, which will supply the correct boundary conditions, T_T and T_B .

(2) Effect of $T_M(\beta)$ Function on Melting Rate

As Fig. 7 illustrates, the slope of T_M versus β (Fig. 5) has a considerable effect on the melting rate. A slower T_M increase

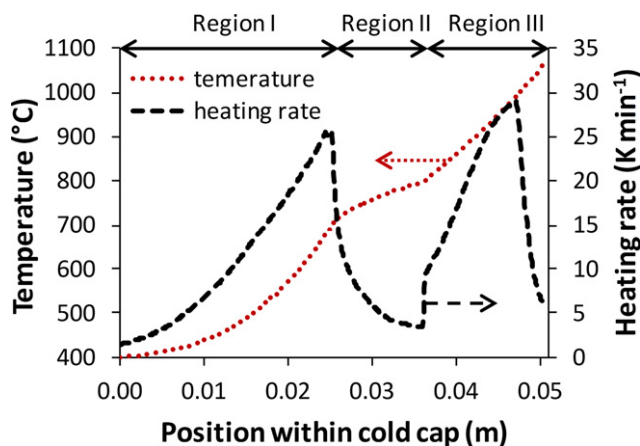


Fig. 8. Temperature and heating rate profiles within the cold cap.

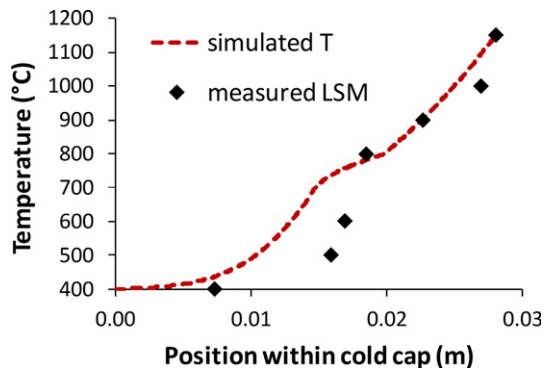


Fig. 9. Comparison of the simulated temperature profile with the profile measured in a cold cap produced in the laboratory-scale melter.

with β (Case A) results in a higher melting rate, as the feed moves faster and experiences a higher heating rate to collapse at the same T_M . An opposite effect is observed for Case B.

(3) Temperature and Heating Rate Profile Within the Cold Cap

Figure 8 displays the temperature and heating rate profiles within the cold cap for a simulation case of $T_T = 400^\circ\text{C}$ and $T_B = 1060^\circ\text{C}$. Three distinct temperature gradient regions can be discerned. In the upper part of the cold cap (Region I), both temperature and heating rate gradually increase with the distance from the cold cap surface. As the increasing temperature approaches the T_P ($\sim 700^\circ\text{C}$ – 800°C , Region II), the heat conductivity of the feed increases as a result of the feed compaction and sintering (Fig. 4). This results in a lower temperature gradient, and thus a decreased local heating rate. Once primary foaming occurs at $\sim 800^\circ\text{C}$ (Region III), the temperature gradient sharply increases, whereas the local heating rate follows the porosity trend displayed in Fig. 3, because the feed moves locally faster when the porosity is higher.

The average heating rate of the feed between 500°C and T_P is 11.6 K/min . At this heating rate, the foam in a pellet collapses at $T_M \approx 1060^\circ\text{C}$ (Fig. 5), identical with the T_B as seen in Fig. 8 at $x = 0.0504\text{ m}$. Note that x is measured from where $Q_T = 0$, while the actual cold cap thickness can extend with a feed of $T_T = \text{constant}$ into an arbitrary negative x value, as seen in Fig. 1(b).

The average heating rate in the primary foam region (between T_P and T_B) was 15.8 K/min , a value close to the average heating rate between 500°C and T_P (11.56 K/min) and within the range of constant heating rate used in the pellet tests. However, the heating rate changed dramatically in the cold cap primary foam (Region III); if the corresponding temperature history were reproduced in the pellet test, the T_M might be affected. Nevertheless, we believe that the identity $T_B = T_M$ provides the best estimate for the $T_B(\beta)$ function based on available data.

(4) Comparison with Experimentally Obtained Temperature Field

Figure 9 displays the cold cap temperature profile in a laboratory-scale melter [Fig. 1(b)] together with the simulated temperature profile. As the temperature profile in the laboratory-scale melter cold cap was only measured after quenching, it was necessary to adjust it to the profile during melting. This was done by assuming that the primary foam layer thickness shrank by 60%. When compared with Fig. 8, the steeper temperature profile in Fig. 9 is caused by the higher T_B in the laboratory-scale melter, resulting in a higher heat flux transferred from the molten glass into the cold cap.

The remaining difference in the measured and simulated temperature profile was likely caused by additional melting and feed compaction during sample quenching.

(5) 3-D melter Model and Future Work

The 1-D cold cap model represents the major part of the 3-D cold cap reasonably well, as long as the field inside the cold cap remains one-dimensional (i.e., if the derivatives of temperature and component velocities with respect to horizontal coordinates are negligible in comparison with those with respect to the vertical coordinate), whereas the boundary conditions are functions of position. This can be expected to be the case except around the vent holes and fissures. To assure the best possible functionality of the combined cold cap–melter model, several phenomena need to be addressed:

1. The formation of vent holes and fissures,
2. Cold cap spreading, and slurry drying in fissures and vent holes, and
3. Molten salt migration and frozen cold cap, suspected to occur in some low-activity waste feeds.³⁹

IV. Conclusions

The mathematical model for the assessment of the melting rate during the vitrification of nuclear waste combines the mass and enthalpy balance of the cold cap together with the conversion kinetics of the feed. The introduction of vigorous bubbling under the cold cap generates powerful forced convection. As a result, the temperature on the most of the cold cap surface can reach up to 400°C while the melt pool currents come into contact with primary foam at the cold cap bottom. In the revised cold cap model, we allowed the top surface temperature to vary, and we identified the bottom temperature with the primary foam collapse temperature, which is a function of the heating rate. This function was determined based on experimental observation of primary foam evolution and decay, for which we developed an empirical relationship that was fitted to the gas phase content data as a function of temperature. The estimates for the melting rate and cold cap temperature profile are in reasonable agreement with data from laboratory-scale and pilot-plant studies. Although the cold cap model inevitably rests on data obtained for a particular waste stream, we believe that the model can be applicable to situations where primary foaming occurs, including commercial glass melting. As the next step, the cold cap model will be validated across a range of feed compositions and incorporated in the glass melter model to relate the feed melting rate to melter operating conditions.

Acknowledgments

This work was supported by the Department of Energy's Waste Treatment and Immobilization Plant Federal Project Office. Richard Pokorny acknowledges financial support from the specific university research (MSMT No 20/2015). The authors are grateful to Jaehun Chun and Dong-Sang Kim for insightful discussions, as well as researchers from the Vitreous State Laboratory of The Catholic University of America for providing cold cap videos. Pacific Northwest National Laboratory is operated for the U.S. Department of Energy by Battelle.

References

- ¹W. S. Kuhn, "Mathematical Modeling of Batch Melting in Glass Tanks"; pp. 73–110 in *Mathematical Simulation in Glass Technology*, Edited by D. Krause and H. Loch. Springer-Verlag, Berlin, 2002.
- ²R. A. Kirkbride, et al., *Tank Waste Remediation System Operation and Utilization Plan, Vol. I, HNF-SD-WM-SP-012*. Numatec Hanford Corporation, Richland, Washington, 1999.
- ³M. K. Choudhary, "Recent Advances in Mathematical Modeling of Flow and Heat Transfer Phenomena in Glass Furnaces," *J. Am. Ceram. Soc.*, **85**, 1030–6 (2002).
- ⁴P. Schill and J. Chmela, "Use of Computer Flow Dynamics in Glass Technology," *J. Non-Cryst. Solids*, **345–346**, 771–6 (2004).

- ⁵C. J. Freeman, *Melt Rate Predictions for Slurry-Fed Glass Melters, PNNL-11012*. Pacific Northwest National Laboratory, Richland, Washington, 1996.
- ⁶R. Pokorny and P. Hrma, "Mathematical Modeling of Cold Cap," *J. Nucl. Mater.*, **429**, 245–56 (2012).
- ⁷R. Pokorny and P. Hrma, "Model for the Conversion of Nuclear Waste Melter Feed to Glass," *J. Nucl. Mater.*, **445**, 190–9 (2014).
- ⁸J. M. Perez, C. C. Chapman, R. K. Mohr, K. S. Matlack, and I. L. Pegg, "Development and Demonstration of an Air Bubbler Design to Meet High-Level Waste Melter Production Rate Requirements of the Hanford Waste Treatment and Immobilization Plant"; In Proceedings for ICEM'05: The 10th International Conference on Environmental Remediation and Radioactive Waste Management, September 4–8, Glasgow, Scotland, 2005.
- ⁹K. S. Matlack, I. L. Pegg, "Advances in JHCM HLW Vitrification Technology at VSL Through Scaled Melter Testing"; pp. 47–58 in *Advances in Materials Science for Environmental and Energy Technologies II: Ceramic Transactions*, Vol. 241, Edited by J. Matyas, T. Ohji, X. Liu, M. P. Paranthaman, R. Devanathan, K. Fox, M. Singh and W. Wong-Ng. Wiley, Hoboken, NJ, 2013.
- ¹⁰M. K. Choudhary, R. Venuturumilli, and M. R. Hyre, "Mathematical Modeling of Glass Melting, Delivery, and Forming Processes," *Int. J. Appl. Glass Sci.*, **1**, 88–214 (2010).
- ¹¹R. Pokorny, A. A. Kruger, and P. Hrma, "Mathematical Modeling of Cold Cap: Effect of Bubbling on Melting Rate," *Ceram.-Silik.*, **58** [4] 296–302 (2014).
- ¹²K. S. Matlack, C. Viragh, W. K. Kot, and I. L. Pegg, *Effect of the Form of Iron on HLW Melt Rate, VSL-15R3430-1*. Vitreous State Laboratory, The Catholic University of America, Washington, DC, 2015.
- ¹³P. Hrma, et al., *Property/Composition Relationships for Hanford High-Level Waste Glasses Melting at 1150°C, PNL-10359, Vol. 1 and 2*, Pacific Northwest Laboratory, Richland, Washington, 1994.
- ¹⁴C. Chapman, *Investigation of Glass Bubbling and Increased Production Rate*, REP-RPP-069, Rev. 0. Duratek, Richland, Washington, 2004.
- ¹⁵J. Wang, B. S. Brewster, M. Q. Mcquay, and B. W. Webb, "Validation of Advanced Models for Glass Melting Furnaces"; pp. 59–76 in *A Collection of Papers Presented at the 60th Conference on Glass Problems: Ceramic Engineering and Science Proceedings*, Vol. 21, Issue 1, Edited by J. Kieffer. John Wiley & Sons, Inc., Hoboken, New Jersey, 2000.
- ¹⁶P. Hrma, "Melting of Foaming Batches: Nuclear Waste Glass," *Glastech. Ber.*, **63**, 360–9 (1990).
- ¹⁷V. Agarwal and D. P. Guillen, *Incorporating Cold Cap Behavior in a Joule-Heated Waste Glass Melter Model*, INL-13-29794. Idaho National Laboratory, Idaho Falls, Idaho, 2013.
- ¹⁸K. S. Matlack, W. K. Kot, R. A. Callow, J. Innocent, and I. L. Pegg, *Testing of Optimized Bubbler Configuration for HLW Melter*, VSL-13R2950-1. Vitreous State Laboratory, The Catholic University of America, Washington, DC, 2013.
- ¹⁹D. Dixon, M. J. Schweiger, B. J. Riley, R. Pokorny, and P. Hrma, "Temperature Distribution Within a High-Level Waste Cold Cap," *Environ. Sci. Technol.*, (2015). doi: 10.1021/acs.est.5b00931.
- ²⁰D. D. Yasuda and P. Hrma, "The Effect of Slurry Rheology on Melter Cold Cap Formation"; pp. 349–359 in *Ceram. Trans. 23: Nuclear Waste Management IV*, Edited by G. G. Wicks, D. F. Bickford and L. R. Brunnell. American Ceramic Society, Westerville, OH, 1991.
- ²¹M. J. Schweiger, P. Hrma, C. J. Humrickhouse, J. Marcial, B. J. Riley, and N. E. TeGrotenhuis, "Cluster Formation of Silica Particles in Glass Batches During Melting," *J. Non-Cryst. Solids*, **356**, 1359–67 (2010).
- ²²P. Hrma, et al., "Effect of Glass-Batch Makeup on the Melting Process," *Ceram.-Silik.*, **54**, 193–211 (2010).
- ²³S. H. Henager, P. Hrma, K. J. Swearingen, M. J. Schweiger, J. Marcial, and N. E. TeGrotenhuis, "Conversion of Batch to Molten Glass, I: Volume Expansion," *J. Non-Cryst. Solids*, **357**, 829–35 (2011).
- ²⁴F. Raether and M. Krauss, "In Situ Measurements of Batch Glass During Melting," *Glass Sci. Technol.*, **77**, 118–23 (2004).
- ²⁵D. S. Kim and P. Hrma, "Volume Changes During Batch to Glass Conversion," *Ceram. Bull.*, **69**, 1039–43 (1990).
- ²⁶D.-S. Kim and P. Hrma, "Foaming in Glass Melts Produced by Sodium Sulfate Decomposition Under Isothermal Conditions," *J. Am. Ceram. Soc.*, **74**, 551–5 (1991).
- ²⁷P. Hrma and D. S. Kim, "Sulfate Mass Balance and Foaming Threshold in a Soda-Lime Glass," *Glass Technol.*, **35**, 128–34 (1994).
- ²⁸R. Pokorny, D. A. Pierce, and P. Hrma, "Melting of Glass Batch: Model for Multiple Overlapping Gas-Evolving Reactions," *Thermochim. Acta*, **541**, 8–14 (2012).
- ²⁹P. Hrma, "Model for a Steady State Foam Blanket," *J. Colloid Interf. Sci.*, **134**, 161–8 (1990).
- ³⁰R. G. C. Beerkens and J. van der Schaaf, "Gas Release and Foam Formation During Melting and Fining of Glass," *J. Am. Ceram. Soc.*, **89**, 24–35 (2006).
- ³¹M. Durand and D. Langevin, "Physicochemical Approach to the Theory of Foam Drainage," *Eur. Phys. J. E*, **7**, 35–44 (2002).
- ³²P. Hrma and S. S. Han, "Effect of Glass Composition on Activation Energy of Viscosity in Glass-Melting-Temperature Range," *J. Non-Cryst. Solids*, **358**, 1818–29 (2012).
- ³³R. Pokorny, J. A. Rice, M. J. Schweiger, and P. Hrma, "Determination of Temperature-Dependent Heat Conductivity and Thermal Diffusivity of Waste Glass Melter Feed," *J. Am. Ceram. Soc.*, **96**, 1891–8 (2013).
- ³⁴J. A. Rice, R. Pokorny, M. J. Schweiger, and P. Hrma, "Determination of Heat Conductivity and Thermal Diffusivity of Waste Glass Melter Feed: Extension to High Temperatures," *J. Am. Ceram. Soc.*, **97**, 1952–8 (2014).
- ³⁵D. P. Guillen and C. J. Beers, *Modeling the Vitrification of Hanford Tank Waste, Transactions of the American Nuclear Society*, Vol. 112. Academic Press, New York, NY, 2015.
- ³⁶H. N. Guerrero and D. F. Bickford, Numerical Models of Waste Glass Melters Part I – Lumped Parameter Analyses of DWPF, WSRC-MS-2003-00272 Part I. Westinghouse Savannah River Co., Aiken, South Carolina, 2003.
- ³⁷H. N. Guerrero, D. F. Bickford, and H. Naseri-Neshat, Numerical Models of Waste Glass Melters Part II - Computational Modeling of DWPF, WSRC-MS-2003-00272 Part II. Westinghouse Savannah River Co., Aiken, South Carolina, 2003.
- ³⁸K. S. Matlack, et al., DM100 and DM1200 Melter Testing with High Waste Loading Glass Formulations for Hanford High-Aluminum HLW Streams, VSL-10R1690-1. Vitreous State Laboratory, The Catholic University of America, Washington, DC, 2010.
- ³⁹P. Hrma, et al., Bulk Vitrification Performance Enhancement: Refractory Lining Protection Against Molten Salt Penetration, PNNL-16773. Pacific Northwest National Laboratory, Richland, Washington, 2007. □